Journal of ELECTRONIC MATERIALS, Vol. 36, No. 12, 2007
DOI: 10.1007/s11664-007-0259-5

*Regular Issue Paper*

# Photothermal Activation of Shallow Dopants Implanted in Silicon

A.T. FIORY,[1,4] A. STEVENSON,[2] A. AGARWAL,[3] and N.M. RAVINDRA[1]

1.—Department of Physics, New Jersey Institute of Technology, Newark, NJ 07102, USA. 2.—Auburn University, Auburn, AL 36849, USA. 3.—Spansion Inc., Sunnyvale, CA 94088, USA. 4.—e-mail: fiory@njit.edu

Dopant impurities were implanted at high dose and low energy ($10^{15}$ $cm^{-2}$, 0.5–2.2 keV) into double-side polished 200 mm diameter silicon wafers and electrically activated to form p–n junctions by 10 s anneals at temperatures of 1,025, 1,050, and 1,075°C by optical heating with tungsten incandescent lamps. Activation was studied for P, As, B, and $BF_2$ species implanted on one wafer side and for P and $BF_2$ implanted on both sides of the wafer. Measurements included electrical sheet resistance (Rs) and oxide film thickness. A heavily boron-doped wafer, which is optically opaque, was used as a hot shield to prevent direct exposure to lamp radiation on the adjacent side of the test wafer. Two wafers with opposing orientations with respect to the shield wafer were annealed for comparison of exposure to, or shielding from, direct lamp illumination. Differences in sheet resistance for the two wafer orientations ranged from 4% to 60%. *n*-Type dopants implanted in *p*-type wafers yielded higher Rs when the implanted surface was exposed to the lamps, as though the effective temperature had been reduced. *p*-Type dopants implanted in *n*-type wafers yielded lower Rs when the implanted surface was exposed to the lamps, as though the effective temperature had been increased. Effective temperature differences larger than 5°C, which were observed for the P, B, and $BF_2$ implants, exceeded experimental uncertainty in temperature control.

**Key words:** Rapid thermal annealing, infrared lamps, temperature, optical process

## INTRODUCTION

Various thermal processes in silicon device fabrication employ heating cycles with short time durations (e.g., from 1 s to 1 min) that are controlled by exposure to photon irradiation and are generally classified as rapid thermal annealing (RTA). Peak heating temperatures are maintained by balancing the heat influx against radiation thermally emitted by the wafer and non-radiative losses through ambient gas convection and conduction. The optical spectrum of the heat source corresponds to an effective temperature that exceeds the wafer temperature by a factor of about 1.2 in a furnace-based RTA method and a factor of about 2 in an incandescent-lamp RTA method. The larger photon energy provided by lamp-based heating methods is believed to be beneficial in the processing of silicon solar cells, for example, when compared to conventional furnace processes.[1] Rapid thermal optical processing with incandescent lamps was shown to be a viable method for junction formation in solar cells.[2] Experimentation with a combination of incandescent and mercury vapor lamps has indicated an increase in dopant diffusion under ultraviolet illumination.[3] Formation of shallow junctions from phosphorus surface diffusion was found to be affected also by exposure to vacuum ultraviolet photons (wavelength $\lambda < 200$ nm).[4] Photonic effects have been studied in a variety of annealing experiments,[5,6] including the electrical activation and diffusion of *n*-type dopants in crystalline silicon.[7] Photonic enhancement with incandescent lamps alone was deduced from dependence on illumination

(Received April 3, 2007; accepted June 11, 2007; published online October 5, 2007)

intensity of the annealing of As and $BF_2$ implant species in silicon wafers.[8,9] Differences between lamp-RTA annealing and conventional furnace annealing have been attributed to lamp photon energies above 1 eV, corresponding to which the radiation is above the Si band gap and is readily absorbed.[10]

Effective diffusion temperatures for phosphorus and boron (but not As) have appeared to be higher in a light-based heating method than in a conventional furnace.[11] The presence of ultraviolet and vacuum ultraviolet photons in RTA processes were also found to improve minority carrier lifetimes in silicon wafers.[12] Low temperature (500°C) nonthermal effects of photo-illumination have been observed in semiconductor surface diffusion[13] and bulk diffusion in silicon.[14]

The work included in the above brief review is a body of evidence with various certainties that an athermal photon flux can influence the RTA process. On the other hand, experiments specifically tailored to discern photonic effects have found no significant enhancement in the activation or diffusion of implanted boron, phosphorus or arsenic in silicon, although analysis has allowed for possible photoeffects in low-temperature processes.[15] Further, studies of the solar cell process found that the presence of ultraviolet photons did not affect the kinetics of dopant diffusion in silicon but did affect the densification of the doped-glass surface film as well as the emissivity of the silicon surface.[16] In another study of the solar cell process, phosphorus was diffused from doped glass deposited on both sides of wafers that were annealed in a lamp-RTA system equipped with excimer ultraviolet lamps in the upper side of the process chamber.[17,18] No significant differences were obtained in the dopant activation on the two sides of the wafers, from which it was concluded that ultraviolet exposure is ineffective for photothermal enhancement. However, such results were deemed to be consistent with any photothermal effect that could be produced by the incandescent lamps themselves.[19]

## EXPERIMENTAL OBJECTIVE

The objective of this paper is to present the results of new experiments that were designed to discern a photothermal effect in dopant activation by comparing an environment of nearly equilibrium photon flux, as in a conventional furnace, with that of excess photon flux inherent to the lamp-based RTA process. A partial furnace-like environment was created on one side of a wafer in a lamp-based RTA system by using a hot shielding wafer in close proximity. The test and shielding wafer assembly were heated simultaneously through an RTA cycle in an incandescent lamp-based RTA system that surrounded the two-wafer assembly with an incident photon flux. Thus, the temperature vs time heating cycle in the illuminated and furnace-like environments were the same. This paper expands upon such an earlier preliminary report.[20]

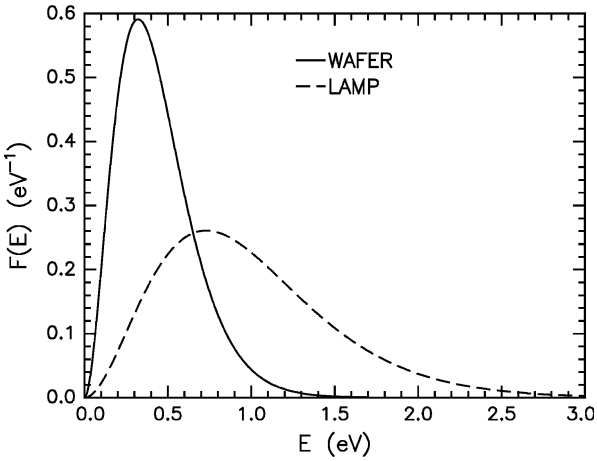


Fig. 1. Planck black body photon energy distributions for a wafer at 1,050°C and lamps at 2,773°C (2,500 K); lamp spectrum multiplied by 0.038.

Figure 1 illustrates black body Planck energy distributions corresponding to a wafer at a temperature of 1,050°C and lamps at 2,773°C. The distribution for the lamps has been scaled by 3.8%, so that the incident lamp energy equals the re-radiated wafer energy and thus corresponds to the steady state energy balance in a rapid thermal process.[21]

## EXPERIMENTAL PROCEDURE

A black body cavity, similar to that in a furnace, was created on one side of a 200 mm diameter test wafer in a lamp-based RTA chamber with dual side heating by placing a heavily doped boron wafer (a blank device grade epitaxial wafer with substrate resistivity <20 mΩ cm), denoted as a shield wafer, in close proximity and heating the two wafers together. The shield wafer is optically opaque in the visible and infrared spectrum throughout the RTA temperature cycle. Sub-band gap radiation is absorbed by extrinsic holes and thermally excited free carriers. Thus, the surface of the test wafer adjacent to the shield wafer was not directly exposed to the heating radiation.

In experiment I, the shield wafer was used as a holder, or susceptor wafer, and the test wafer was placed on top of it, with three L-shaped quartz spacer pins in-between the shield wafer and the test wafer. This created a black body-like cavity within a 2 mm gap at the lower surface of the test wafer. The two-wafer assembly was heated in a lamp-based RTA chamber as illustrated in Fig. 2. The RTA system is an AG Associates model 8108, equipped with a power line regulator and an emissivity-compensating ripple pyrometer that are used to control the temperature of the bottom wafer.[22] The chamber

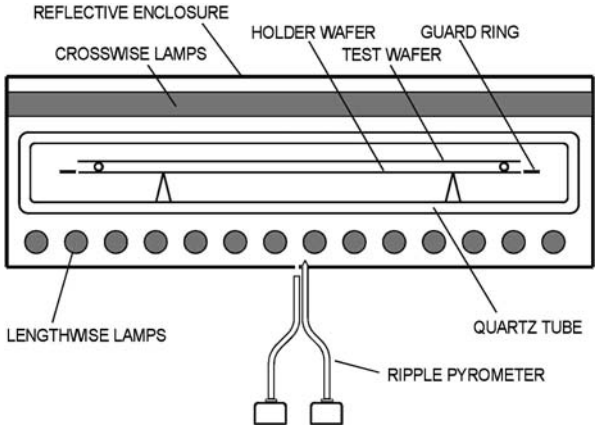


Fig. 2. Schematic cross-section of the oven in the AG Heatpulse rapid thermal annealing system with two-wafer assembly for experiment I. A 2 mm gap between wafers is exaggerated for clarity. Not shown: quartz tray detail.

contains an annular guard ring comprised of SiC coated with polycrystalline Si for the improvement of temperature uniformity. Wafers are heated by upper and lower arrays of tungsten incandescent lamps, with power distribution adjusted for optimal uniformity of wafer temperature in the test wafer (within ±5°C). Temperature was also passively monitored by a thermocouple probe in contact with the lower wafer at the rear of the RTA oven. The centroid of the ripple pyrometer view area is located 25 mm from the wafer center at a 126° polar angle relative to the rear of the oven. Experiment I tested single side implant anneal, in which a pseudo-black body environment is created below the test wafer.

Experiment II consisted of anneal of implanted wafers, in which the shield wafer was placed on top of the test wafer, separated by quartz pins, so that the pseudo-black body environment was created on the upper surface of the test wafer. The ripple pyrometer controlled the temperature of the test wafers directly. The test assembly for experiment II is illustrated in Fig. 3.

The test wafers were annealed for 10 s RTA at temperatures of 1,025, 1,050 and 1,075°C in $N_2$ with 0.1% $O_2$ (for suppressing dopant outgas). Ramp-up rate was programmed at 40°C/s. Ramp-down rate was programmed at 100°C/s. Wafers were oriented with the alignment notch at the rear of the oven, located opposite the entry door. A dummy wafer was

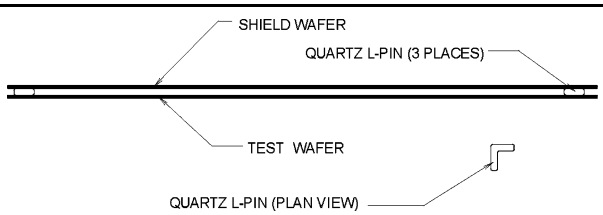


Fig. 3. Two-wafer assembly for experiment II. Implanted test wafer is on the bottom. Epi-cover wafer is on top, spaced off by three quartz L-pins, shown in the profile.

**Table I. Annealing Test Sequence for Six Test Wafers of a Given Type**

| Step | Wafer | Orientation | Temperature (°C) |
|---|---|---|---|
| 1 | Dummy | Up | 1,025 |
| 2 | Test | Up | 1,025 |
| 3 | Test | Down | 1,025 |
| 4 | Test | Up | 1,050 |
| 5 | Test | Down | 1,050 |
| 6 | Test | Up | 1,075 |
| 7 | Test | Down | 1,075 |

Orientation "up" denotes that wafer's front side (the scribed side) was loaded facing up; "down" denotes that the front side is facing down.

mounted in the assembly and annealed before performing the experiments on test wafers. The dummy and a group of six identically prepared test wafers were annealed without interruption in a semi-automated operation with robotic loading and unloading of the two-wafer assembly. Robot motion was programmed to be slower than normal, so that the top wafer did not slip during the loading and unloading processes. The sequence of the annealing steps is listed in Table I. Each annealing step is preceded by the preheating of the RTA oven, with the lamps operated at 40% of maximum intensity. Lamp power, which is under closed loop ripple pyrometer control during the annealing of the wafers, is in the range of 45–50% during the 10 s anneal period. The time for mounting the two-wafer assembly, preheating the oven, transporting the wafer, annealing the wafer, cooling, and disassembling comprised an 8 min cycle that was held constant for each RTA test. Such a protocol reproduced background sources of residual heat from one RTA test to the next. In order to minimize temperature uncertainties that may arise from surface finish on the wafers, the experiments employed double-side polished *p*- and *n*-type 200 mm diameter Si wafers.

After the anneals, sheet resistance, Rs, was mapped at 127 points by a CDE ResMap scanning four-point probe system. The mapping pattern allocates a constant area per point. Edge exclusion was 6 mm. Probe type was equivalent to Prometrix D: 0.5 mm tip radius, 1 mm tip spacing, 100 g loading. The ResMap system checks for ohmic probe contact with the wafer, and the software produces contour plots showing Rs mean and standard deviation and wafer identification.

## EXPERIMENTAL

The wafers and implants for experiment I are listed in Table II. The reverse sides were implanted first, followed by a clean, and then a second, implant on the front sides. The front sides were inscribed with wafer identification numbers. The intention of our having the wafer cleaned was to reduce particle

**Table II. Implanted Wafers for Rapid Thermal Annealing Experiment I**

| Wafer Type | Implant Species | Energy (keV) | Dose ($cm^{-2}$) |
|---|---|---|---|
| p | P | 1 | $10^{15}$ |
| p | As | 2 | $10^{15}$ |
| n | $^{11}B$ | 0.5 | $10^{15}$ |
| n | $BF_2$ | 2.2 | $10^{15}$ |

accumulation. However, the cleaning also removed some of the implant dose as well, so those wafers were treated as front side test implants.

In experiment I the top surface of the test wafer was exposed to the lamp radiation, while the bottom surface of the test wafer was shielded by the holder wafer. The radiation environment at the bottom surface of the test wafer was similar to that of black body cavity, because numerous multiple reflections between the shield and test wafer yielded effective surface emissivities of unity. The temperature of the holder wafer was controlled by the ripple pyrometer. Two test wafers, each with an implant type given in Table II, were annealed at each temperature, one with the implanted test surface exposed to the lamp radiation (denoted "exposed") and the other with the implanted test surface shielded from the lamp radiation (denoted "shielded"). The temperature of the test wafer was estimated from separate experiments to be within ±5°C of that of the holder wafer. The temperature difference between the holder and test wafers was estimated to vary by fewer than 2°C, owing to emissivity changes of 0.02, caused by the implants, and from reproducibility of the lamp power in closed-loop control, which varied randomly within a ±0.5% range. The temperature difference across the thickness of the test wafer was less than 1°C.

## Results of Experiment I

By design, the dopant and wafer were of opposite types, so that *p-n* junctions were formed in the annealed wafers, isolating the electrical activation of the surface from the substrate. The sheet resistance, Rs, of the wafers was measured at 127 points with 6 mm edge exclusion by the scanning four-point probe. The mean of seven Rs measurements inside a central circle of 16.7 mm radius is shown as a function of annealing temperature in Fig. 4. Data are presented for the four implant types and are distinguished as to whether the test implant surfaces were exposed to, or shielded from, the lamps. These results show that exposure to lamp radiation leads to larger Rs for the *n*-type dopants and smaller Rs for the *p*-type dopants, when compared to Rs corresponding to shielding from lamp radiation. Figure 5 shows sheet resistance contour maps in the case of the P and $BF_2$ implant anneals at 1,025°C for 10 s. The means and standard deviations of the sheet resistance maps are shown in Table III.

The variation of Rs with annealing temperature was used to associate a change in the effective process temperature with a change in Rs. Using this approach, the results in Fig. 4 can be interpreted as follows: the presence of lamp illumination is equiv-

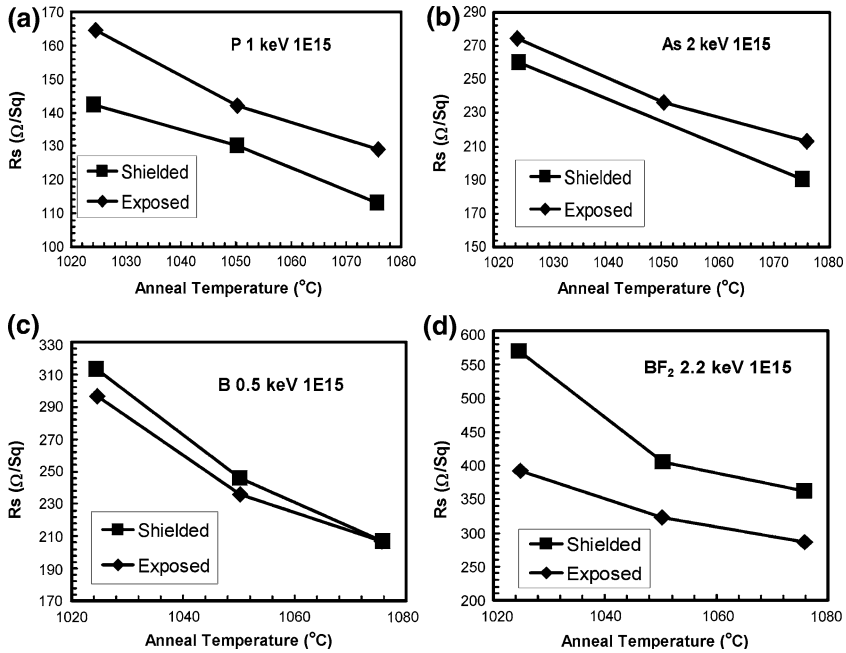


Fig. 4. Experiment I mean sheet resistance Rs within a 16.7 mm radius of wafer center as function of annealing temperature. Squares represent anneals with exposure to lamp illumination; diamonds represent anneals shielded from lamp illumination. The implants are as indicated in the legends.

**Table III. Mean and One Standard Deviation for Sheet Resistance Rs Obtained from 127-Point Probe Maps with 6 mm Edge Exclusion for Wafers of Experiment I Annealed at 1,025°C for 10 s**

| Implant Species | Exposed or Shielded | Mean Rs (Ω/sq) | 1-σ Rs (Ω/sq) |
|---|---|---|---|
| P | Exposed | 158.9 | 3.3 |
| | Shielded | 135.5 | 3.0 |
| As | Exposed | 270.5 | 3.3 |
| | Shielded | 257.9 | 3.9 |
| B | Exposed | 296.3 | 6.7 |
| | Shielded | 310.0 | 6.1 |
| $BF_2$ | Exposed | 392.4 | 6.6 |
| | Shielded | 570.4 | 68.5 |

Exposed or shielded refers to implanted and probed surfaces.

alent to reducing the anneal temperature by 10°C for the P implants and 5–7°C for the As implants. This is equivalent to increasing the anneal temperature by up to about 5°C for the $^{11}B$ implants and 50°C or more for the $BF_2$ implants.

The "exposed" and "shielded" Rs contour maps for various implants turn out not to be mirror symmetric (e.g., Fig. 5), as might be expected if all the Rs variation were produced as an imprint of the heating pattern that is characteristic of the RTA system. Since Rs depends on both temperature and lamp illumination, the Rs contour maps are not absolute measures of wafer temperature uniformity, in contrast to a conventional interpretation of how implant monitors may assess process uniformity. In this RTA system, temperature uniformity is determined by fixed fractions of power distributed among the lamps. As is typical for lamp-based systems, the illumination pattern is deliberately non-uniform, because the lamp power distribution is tuned for

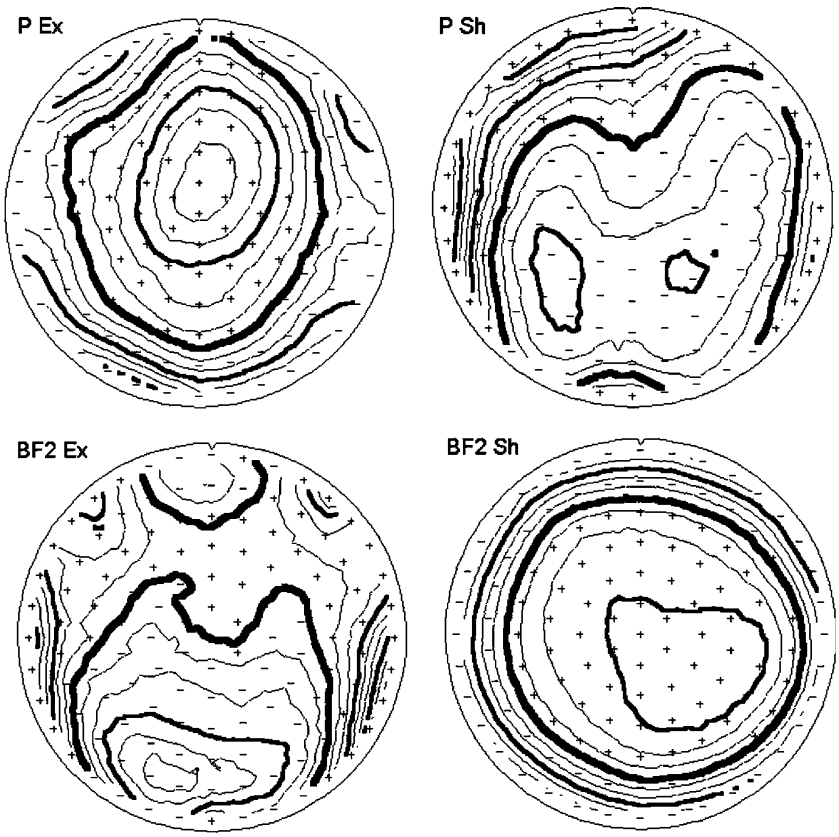


Fig. 5. Experiment I sheet resistance contour maps from 127-point measurements with 6 mm edge exclusion, for wafers implanted with P and $BF_2$ and annealed at 1,025°C for 10 s. "Ex" denotes test surface exposed to lamp illumination, "Sh" denotes test surface shielded from lamp illumination. Heavy contours correspond to mean Rs; contour separation is 1/3 standard deviation. Means and standard deviations are given in Table III.

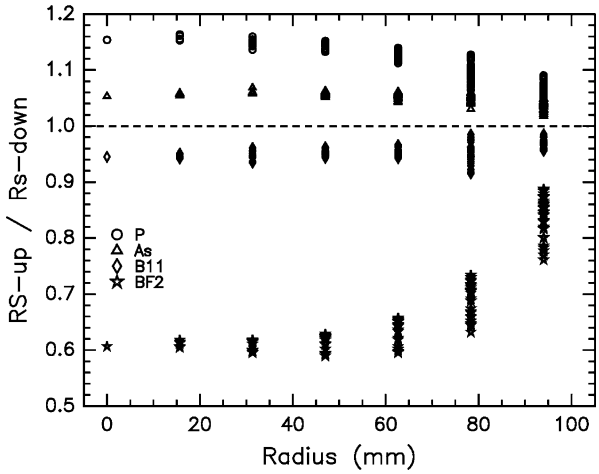


Fig. 6. Experiment I ratios of the sheet resistance, Rs, for wafers exposed to lamp radiation to the Rs for wafers shielded from lamp radiation, as a function of radial coordinate. Implants are P, As, $^{11}B$, and $BF_2$ (indicated as P, As, B11, and BF2, respectively). Dashed line denotes unity ratio.

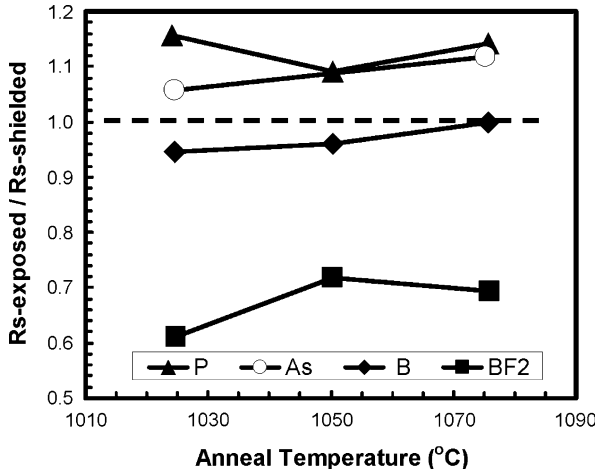


Fig. 7. Experiment I ratios of mean Rs (within a 16.7 mm radius of wafer center) for wafers exposed to lamp radiation to mean Rs for wafers shielded from lamp radiation, as a function of anneal temperature. Implants are P, As, $^{11}B$, and $BF_2$ (indicated as P, As, B11, and BF2, respectively). Dashed line marks unity ratio.

optimum process uniformity. The lamp power profile compensates for the finite sizes of the wafer and the chamber. Results such as in Fig. 5 imply that the lamp power distribution, which minimizes the variation in Rs across the wafer, does not necessarily minimize the temperature variation across the wafer (and vice versa). For example, in lamp-based RTA systems that use multipoint temperature sensing to assure temperature uniformity, one generally needs to apply an offset distribution within the feedback control system that is tailored to fine-tune uniformity in a wafer for a particular process.

The change in the appearance of the contour maps when the test surface was exposed or shielded is largely due to different radial dependences of Rs for the two orientations. This is illustrated in Fig. 6, in which ratios of Rs from "exposed" and "shielded" 127-point maps are plotted versus the radial coordinate (the angular coordinate is mirrored in the calculations, since "exposed" orientation is flipped with respect to "shielded"). For the P and As implants, which were *n*-type dopants in *p*-type wafers, the ratio is greater than unity near the center of the wafer and decreases with radius, approaching unity near the edge of the wafer. For the $^{11}B$ and $BF_2$ implants, which were *p*-type dopants in *n*-type wafers, the trends are opposite: the ratio is less than unity near the center of the wafer and increases towards unity near the edge of the wafer. The radial dependence can be attributed to lamp radiation entering along the perimeter of the gap between the test and holder wafers. The RTA system uses an edge guard ring, which is in the plane of the holder wafer. Consequently, the periphery of the test wafer surface is exposed to lamp radiation, even in the "shielded" orientation. Thus, the shield wafer can contribute to non-uniformity in the process results because the edge of the wafer remains partially exposed.

The photo-effect of the radiation guided between the wafers appears to have a range of about 50 mm and becomes completely attenuated inside the 16.7 mm radius from the wafer center. Data from the area near the wafer center are, therefore, most representative of the presence or absence of the lamp illumination effect and, thus, were used for the analysis in Fig. 4. The attenuation length of the photo-effect, which is about eight-times the gap between the test and shield wafers, is consistent with the attenuation of the photon flux by wafer absorption (absorptivity $\sim$0.65).

Figure 7 summarizes the results for the four implants. It shows the temperature dependence of the ratio of the mean Rs within a 16.7 mm radius for the "exposed" and "shielded" wafers. The lamp illumination effect (indicated as deviation from unity) is most pronounced for the $BF_2$ implant.

## Summary of Experiment I

Silicon wafers were implanted with P, As, $^{11}B$, and $BF_2$ at high doses and low energies. The implanted surface was either exposed to, or shielded from, incandescent lamp radiation in rapid thermal annealing. *n*-Type dopants showed lower activation when the implanted surface was exposed to the lamps, as though the effective temperature had been reduced by 5–10°C. *p*-Type dopants showed higher activation when the implanted surface was exposed to the lamps, as though the effective temperature had been increased by 5–50°C. Differences larger than 5°C are experimentally meaningful, as they are greater than the uncertainty in the reproducibility of temperature control.

The RTA of shielded wafers resulted in edge effect patterns in the sheet resistance. The magnitude of this wafer-scale pattern effect was most pronounced for P and $BF_2$ implant anneals and was correlated with exposure to lamp illumination. The use of proximity shields to reduce temperature variation patterns in RTA processes has been studied previously.[23,24] However, this earlier work was concerned only with the issue of emissivity patterns on the wafer.[21] Process variability with photonic illumination were not explicitly considered when the behavior of a hot shield was evaluated in earlier work.

## EXPERIMENT II

Based on the findings in experiment I, a second set of wafers was prepared for the further testing of the influence of incandescent lamp radiation on the electrical activation of shallow ion implants of $^{11}B$, $BF_2$, and P species, in which the evidence is clearer that exposure to lamp radiation increases the electrical activation of B and reduces the activation of P. Double side polished 200 mm diameter wafers were implanted in both sides with P (1.0 keV, $10^{15}$ $cm^{-2}$) in *p*-type wafers and $BF_2$ (2.2 keV, $10^{15}$ $cm^{-2}$) in *n*-type wafers. The cleaning step after implantation in the first experiment was not used, in order to preserve the implant dose. Additional *n*-type double-polished wafers were implanted in the front side only, with $^{11}B$ (0.5 keV, $5 \times 10^{14}$ $cm^{-2}$). Wafer sides inscribed with identification numbers were denoted as the "front" side and the opposite sides as the "back" side. The implanted test wafers were covered in the RTA oven with a shield wafer to block lamp radiation from directly reaching the top surface, using the assembly shown in Fig. 3. Wafers with the $^{11}B$ implants and clean bare monitors were used to determine the optimum fixed lamp power distribution for best process uniformity, by mapping sheet resistance or oxide thickness. Test wafers were oriented either front side up or front side down and received 10 s RTA at 1,025, 1,050, or 1,075°C, during which the wafer temperature was controlled directly by the ripple pyrometer system.

### Temperature Dependence

The mean Rs in the center of the wafer was obtained by averaging sheet resistances at seven probe points within a 16.7 mm radius. The results are plotted as functions of anneal temperature in Fig. 8. Measured sides of the wafers are designated in the figure legends by "F" for front side and "B" for back side in the double-side P and $BF_2$ implants. The two orientations of the wafers in the RTA are distinguished according to whether the measured side was shielded from, or exposed to, direct incidence of lamp radiation. The results of Fig. 8 are qualitatively similar to those obtained for experiment I in Fig. 4. Exposure to lamp illumination reduces phosphorus activation and increases boron activation.

### Photothermal Effective Temperatures

Sheet resistance data for experiment II were analyzed in terms of the change in effective anneal temperature that may be attributed to exposure to

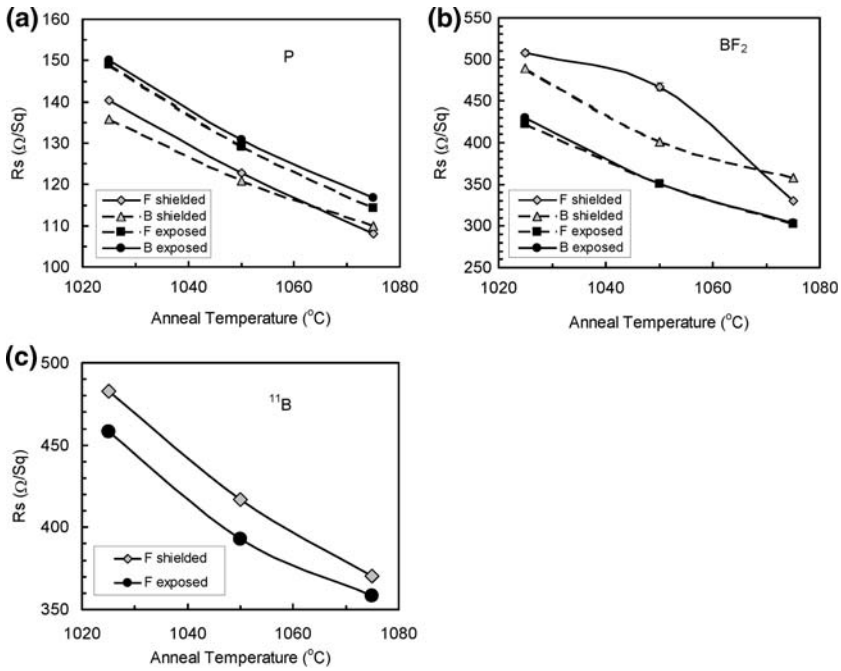


Fig. 8. Experiment II mean of sheet resistance Rs within a 16.7 mm radius of wafer center as a function of annealing temperature. F denotes measurement of the front side of the wafer and B denotes measurement of the back side of the wafer. Symbols indicate whether the measured side was shielded from, or exposed to, direct lamp radiation.

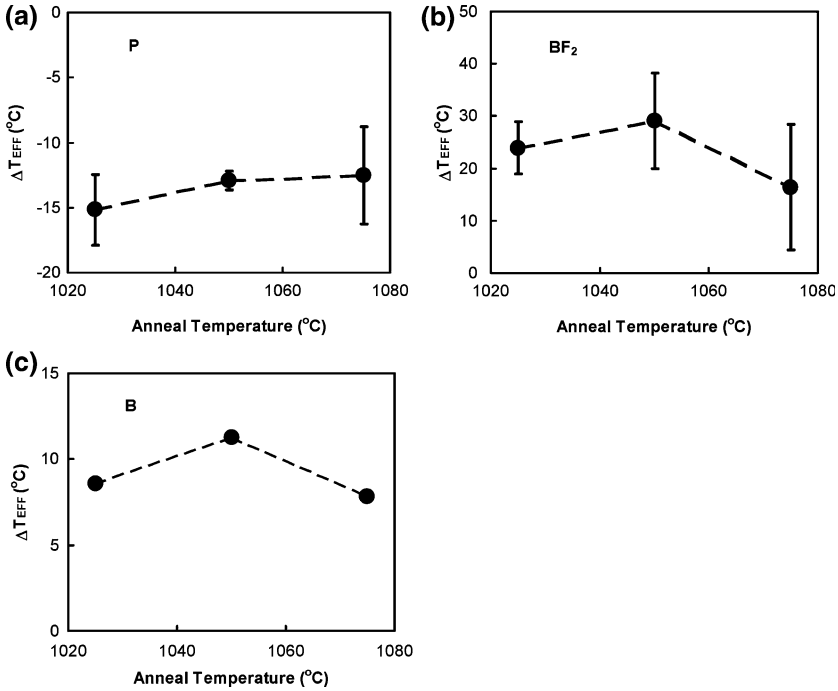


Fig. 9. Change in effective process temperature of P, $BF_2$ and $^{11}B$ implants associated with lamp illumination; results of experiment II.

lamp illumination. They quantify observations of differences between an effective photothermal temperature and the thermodynamic temperature within the pseudo-black body environment. A change in the effective anneal temperature, $\Delta T_{EFF}$, is defined as the difference in Rs of wafers with the implanted surfaces exposed and those with the implanted surfaces shielded, divided by the coefficient of temperature sensitivity, $\Delta Rs/\Delta T$, obtained from the local slope of the experimental data for Rs versus anneal temperature.

The results for $\Delta T_{EFF}$ for the three implant species at the three RTA temperatures are shown in Fig. 9. The data points correspond to the mean $\Delta T_{EFF}$ for the two wafer orientations. The error bars span the difference between the two orientations. (The data for the B implant are without error bars, owing to the single-side implant method used for that case.)

Table IV presents the results for $\Delta T_{EFF}$ averaged for the three RTA temperatures. One finds that $\Delta T_{EFF}$ is decreased for the *n*-type phosphorus dopant and is increased for the *p*-type boron dopant.

**Table IV. Difference Between Effective Rapid Thermal Annealing Temperatures Under Exposure to Lamp Illumination, Relative to Being Shielded, for the Three Implants in Silicon Studied in Experiment II**

| Implant | $\Delta T_{EFF}$ (°C) | $\pm\Delta T_{EFF}$ (°C) |
|---|---|---|
| P 1.0 keV $10^{15}$ $cm^{-2}$ | –15.5 | 1.4 |
| $BF_2$ 2.2 keV $10^{15}$ $cm^{-2}$ | 23.1 | 6.4 |
| $^{11}B$ 0.5 keV $5 \times 10^{14}$ $cm^{-2}$ | 9.2 | 1.8 |

## Radial Rs Scans

The variation in sheet resistance along the radial direction at a polar angle of 120° relative to the wafer alignment notch is shown for the P implant in Fig. 10 and for the $BF_2$ implant in Fig. 11. The data correspond to RTA at 1,050°C. Sheet resistance is scanned from the wafer center out to the wafer's edge, crossing the approximate location of the ripple pyrometer view area at 25 mm from the wafer center. In experiment II, the guard ring is in the plane of the wafer, and, being also thicker than the wafer, it shades the lamp illumination at the edge of the shielded surface of the test wafer more effectively than in the configuration of experiment I, in which the edge of the test wafer lies above the plane of the guard ring.

Sheet resistivity scans for both sides of the same wafer are shown in Figs. 10 and 11. Data are plotted for the two wafer orientations (a) front side up and (b) front side down. "F" denotes measurement of the front side of the wafer; "B" is the back side. "Shielded" denotes that the measured implanted side is oriented up and shielded from the lamps by the cover wafer. "Exposed" denotes that the measured implanted side is oriented down and exposed to the lamps. The edge illumination effects displayed by the data of Fig. 11 for the $BF_2$ and $^{11}B$ implants (not shown) are similar to the observation in Fig. 6, in that Rs at the wafer edge for the shielded and exposed surfaces are nearly the same. An edge effect

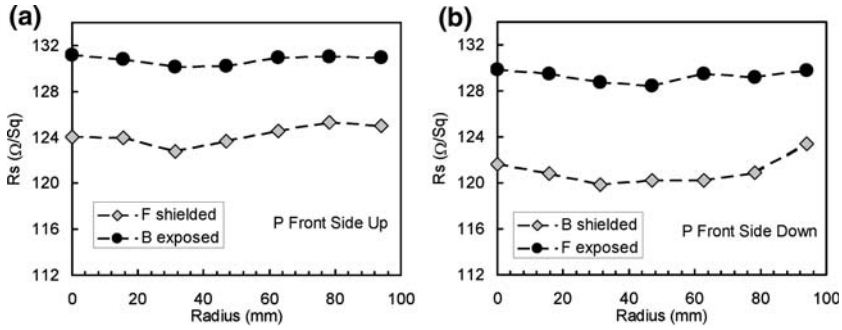


Fig. 10. Radial scan of sheet resistance for P-implanted wafers oriented (a) front side up, (b) front side down, in experiment II.

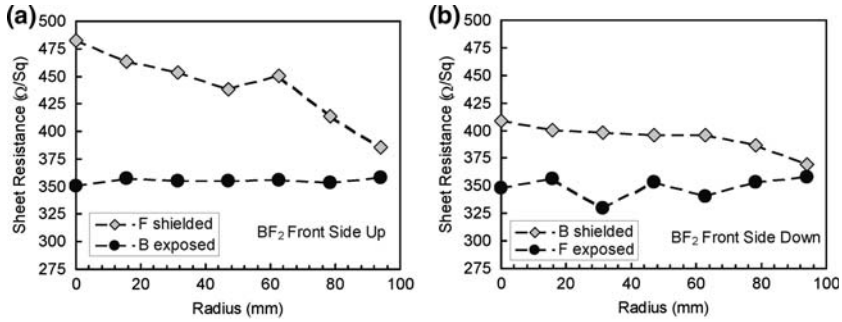


Fig. 11. Radial scan of sheet resistance for $BF_2$-implanted wafers oriented (a) front side up, (b) front side down, in experiment II.

is hardly discernable in the case of the P implant. This may indicate that electrical activation for the phosphorus implant is less sensitive to illumination than that for the boron implants.

The sheet resistance data indicate systematic differences between the wafers annealed with the front side up and those with the front side down. These differences may have been due to (a) surface preparation of the two sides of the wafers by the wafer vendor or (b) the implants. While wafer-to-wafer differences contributed to the experimental error in the results for $\Delta T_{EFF}$, the differences associated with exposure to and shielding from the lamp illumination were, nevertheless, clearly distinguished in experiment II. The quantitative analysis of these experimental results is discussed below.

## Wafer Oxidation

Oxide films grown during the RTA process were mapped with a Thermawave scanning ellipsometer and were interpreted as comprising $SiO_2$ due to thermal oxide on silicon. The film thickness results were consistent with penetration of the four-point resistance probe through the oxide. Mean and standard deviation of the oxide film thickness at 12 probe points near the center of the wafers are shown in Fig. 12 for the P-, $BF_2$- and, $^{11}B$-implanted wafers. The back sides of the $^{11}B$-implanted wafers were not implanted with any dopants. The thicker oxide film found for the implanted side of the $^{11}B$ wafers could indicate a residue of the implant or a systematic measurement error, since the effect of boron doping was not taken into account in the ellipsometry model. For P- and $BF_2$-implanted wafers, oxides on the exposed sides were systematically thinner than on the shielded side. The average differences in oxide thickness (shielded side versus exposed side) for the P, $BF_2$ and $^{11}B$ implants were 3 ± 1 Å, 6.7 ± 1 Å, and 1 ± 2 Å, respectively.

The question of whether the growth of the oxide film depends on the wafer type was examined in a separate experiment in which 12 *n*-type and 12 *p*-type wafers were subjected to rapid thermal oxidation (RTO). The wafers were prime, single-side, polished wafers that had been given a pre-gate clean [a metal-oxide-semiconductor (MOS) device process] with HF in the last step. The cleaning process leaves the surfaces of the wafer stripped of the oxide (as determined by ellipsometry) and in a hydrophobic state. The cassette of 24 wafers was immediately loaded for RTO without delay. The RTO was a 1,000°C reduced $O_2$ pressure process in an Applied Materials' Centura with multipoint zone temperature control and wafer rotation. After oxidation, the *p*-type wafers in slots 6 and 12, and the *n*-type wafers in slots 18 and 24, were removed for oxide thickness mapping. The experiment was then repeated. (In the second run, there was a 2 h delay between RTO and measurement.) The results of these two experiments, denoted as run A and run B, are shown in Fig. 13. Oxide films grown on *n*-type wafers were systematically larger than those grown

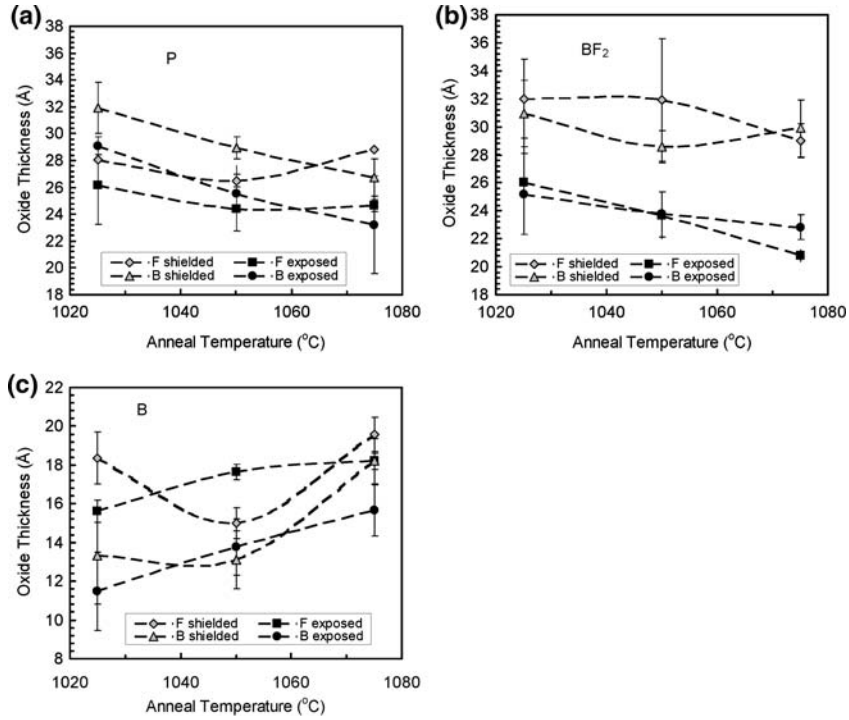


Fig. 12. Thickness of oxide grown on (a) P-implanted wafers, (b) $BF_2$-implanted wafers in experiment II. "F" denotes measurement of the front side, "B" denotes measurement of the back side; the measured side was shielded or exposed. The points are connected to guide the eye.

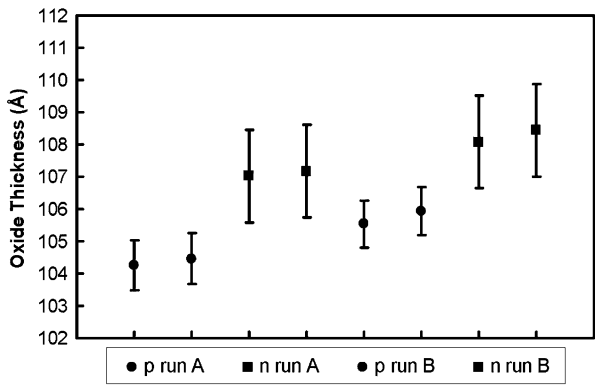


Fig. 13. Thickness of oxide grown on clean p- and n-type wafers by rapid thermal oxidation. Experiment repeats are denoted as "run A" and "run B".

on *p*-type, by two standard deviations, as determined by within-wafer variations of the oxide film thickness. Uniformity for the *n*-type wafers is worse, probably because wafer uniformity of the RTO process had been tuned for *p*-type wafers.

## Summary of Experiment II

Exposure to lamp illumination increased Rs by 7% to 9% for P implants. The changes in Rs were equivalent to the anneal temperature's being decreased by 15.1 ± 1.4°C. Exposure to lamp illumination reduced Rs by 3% to 6%, for $^{11}B$ implants, and 9% to 28% for $BF_2$ implants. The changes in Rs are equivalent to the anneal temperature's being increased by 9.2 ± 1.8°C and 23.1 ± 6.4°C, respectively. Sheet resistances on the sides of the wafers that were exposed to the lamps were reproducible to about 2% for both $BF_2$ and P implants. Sheet resistances on the sides of the wafers that were shielded from the lamps were less reproducible, showing variability of 4% to 15% for $BF_2$ implants and 2% to 4% for P implants. The $^{11}B$ and $BF_2$ implants showed pronounced radial dependence in the difference in Rs between the shielded and exposed sides. The magnitude of this difference in Rs depended on proximity of the measurement sites to the wafer edge, where it is a minimum. Radial dependence was caused by the gap between the test and shielding wafers that permitted some lamp radiation to interact with the wafer at the wafer edge. The P implants showed less radial variation in the difference in Rs between the shielded and exposed sides. The greater variability in the Rs for the shielded sides for the $BF_2$ implants appeared to be correlated with the increased sensitivity to lamp exposure, as evidenced by the more pronounced radial variation.

Ellipsometric thickness of oxide films grown on implanted wafers appeared to be decreased under lamp exposure, irrespective of either dopant or wafer type, when exposed and shielded configurations were compared. In the case of P-implanted wafers, illumination appeared to reduce oxide thickness by 11 ± 3%. For the $BF_2$-implanted wafers, the oxide

thickness effect was larger, averaging 25 ± 3%. The apparent independence of the sign of the oxide thickness effect stands in contrast to that of the sheet resistance, in which the sign depended on dopant/wafer type. Small differences in oxide thickness between *n*-type and *p*-type wafers are possible, based on RTO studies of unimplanted clean wafers.

## DISCUSSION OF RESULTS

Implant energies in this study were sufficiently low to permit formation of the activated impurity layer within the region of penetration of lamp illumination. Based on the studies of optical absorption in Si at elevated temperatures,[25] the optical penetration depth is of the order of 100 nm. The depths of the electrically activated layers after rapid thermal annealing were estimated from sheet resistance and dopant concentration profiles that had been determined in previous work by secondary ion mass spectroscopy.[26–30] The depth to which the dopants diffuse after RTA is defined by a junction depth parameter, $X_J$, which is defined as the depth at which the dopant volume concentration falls to $10^{18}$ cm$^{-3}$. For a given implant species, energy and dose, the product Rs $\times X_J$ tends to be insensitive to variations in the annealing conditions and can thus be used to find $X_J$ for the present Rs data by interpolation (±20% estimated uncertainty). Estimates of $X_J$ for experiment I, based on prior studies for the annealing of P,[26] As,[27] $BF_2$,[28,29] and B[30] implants, are shown in Table V. Junction depth analysis thus affirms that the activated layers are generally shallower than the depth of penetration of the heating radiation.

Differences in apparent photothermal activation among the various dopant species in this work might be connected with the nature of their electrical activation behavior. Diffusion and electrical activation of the implanted dopant species in silicon by rapid thermal annealing exhibit significant nonequilibrium and transient behavior, caused by the formation and evolution of defects associated with implant damage and high dopant concentrations. Transient enhanced diffusion is observed for boron and phosphorus implants, owing, in part, to the presence of silicon interstitials.[31] The transient diffusion of arsenic implants involves vacancies and is generally less of an effect. Thus, the larger photothermal effects observed for boron and phosphorus may be associated with their more pronounced transient enhanced diffusion that is associated with silicon interstitials.

**Table V. Junction Depths of Implants at $10^{15}$ cm$^{-2}$ Dose After 10 s Rapid Thermal Annealing at 1,050°C Under Exposure to Lamp Illumination**

| Implant | $X_J$ (nm) |
|---|---|
| P 1 keV | 53 |
| As 2 keV | 41 |
| $BF_2$ 2.2 keV | 53 |
| B 0.5 keV | 89 |

In order to interpret the results of sheet resistance, it is instructive to consider earlier findings of the electrical activation process, within which transient diffusion is a constituent physical mechanism. Of particular interest is the observation of a phenomenological thermal activation energy, $E_A$, that is associated with the electrical activation of the dopant impurities. Using Hall effect measurements to monitor relationships between annealing temperature and annealing duration, previous work has found that $E_A$ for the *n*-type impurities is smaller by about 1 eV than that of the *p*-type, $E_A$ being 4.1, 4.9, and 4.7 eV for P, $BF_2$ and B, respectively.[32] Detailed study in the case of boron found that the $E_A$ for electrical activation exceeds the corresponding $E_A$ for thermal diffusion by about 1 eV.[33] Our observation of a decrease in electrical activation of phosphorus upon photon exposure supports the idea that the associated $E_A$ increases. Converting the apparent temperature shifts in Table IV to changes in activation energy according to the relationship $\Delta E_A/E_A = -\Delta T_{EFF}/T$, one obtains a photothermal increase in $E_A$ by 1.2% for the annealing of the P implant. Increased electrical activation of boron under illumination is equivalent to decreases in $E_A$ by 1.7% for the $BF_2$ implant and 0.7% for the B implant. Activation energies, therefore, are changed by 0.03–0.08 eV under photo-illumination. Moreover, photoexposure causes the 1 eV difference in $E_A$ between these *n*-type and *p*-type species to shrink by several percent. These results suggest the presence of a solid-state photochemistry component in the lamp-based RTA process.

While the values of $E_A$ for boron, as determined under illumination, are about the same for both B and $BF_2$ implants, the $BF_2$ species shows a stronger photo-effect. Even though the heavier F species creates more implant damage than does B alone, there is less boron diffusion for $BF_2$ implants, as indicated by generally smaller $X_J$, because fluorine reacts with silicon interstitials and partly suppresses the transient enhanced diffusion.[34] The result suggests that $\Delta E_A$ for $BF_2$ implants is larger than for B implants because of additional reaction pathways involving F impurities.

At an annealing temperature of 1,050°C, the intrinsic carrier concentration in silicon increases to about $n_I \approx 2 \times 10^{19}$ cm$^{-3}$.[35] From Ref. 35, the temperature coefficient of $n_I$ is calculated to be $\alpha = \mathrm{d} \ln n_I/\mathrm{d}T = 0.0071$ K$^{-1}$. Since $n_I$ is smaller than the peak dopant concentrations, which exceed $10^{20}$ cm$^{-3}$, an extrinsic surface layer is formed in the silicon wafer at the annealing temperature. Making the assumption that lamp illumination changes $n_I$ by fraction $\Delta n_I/n_I = \alpha|\Delta T_{EFF}|$ through electron–hole pair generation, while actual wafer temperature remains unchanged, the results in Table IV

indicate a $\Delta n_I/n_I$ of 0.11, 0.17 and 0.66 for the P, $BF_2$ and B implants, respectively. Effective changes in Fermi energy calculated for the extrinsic approximation, $\Delta E_F = k_B T\ \Delta n_I/n_I$, are −0.012, 0.018, and 0.007 eV for the P, $BF_2$ and B implants, respectively. This interpretation of the results suggests that the energy scale of the perturbations produced by lamp illumination is about 0.01 eV, which is about 1% of the silicon energy gap at 1,050°C, $E_g$ 1.04 eV.[35] Note from Fig. 1 that the lamps supplied significant energy in the region $E > E_g$, when compared to the thermal equilibrium background at wafer temperature.

Oxide growth is found to be affected by lamp illumination, which yields thinner oxides, particularly in the case of the $BF_2$ implant. Oxidation injects silicon interstitials, which ordinarily accelerates dopant diffusion.[36] However, the presence of interstitials generated within the silicon, such as from lamp illumination, could reduce oxidation by mass action.

## CONCLUSIONS

Electrical activation of shallow high-dose implants by rapid thermal annealing was found to depend on exposure to lamp illumination. Changes in sheet resistance were interpreted in terms of changes in either effective wafer temperature or a phenomenological activation energy. Formation of donors with *n*-type implants of P or As is reduced, while formation of acceptors with *p*-type implants of B or $BF_2$ is increased. Lamp illumination increases the thermal activation energy for the formation of electron carriers and decreases it for holes. Lamp illumination has the equivalent effect of modulating Fermi levels on the order of 0.01 eV. Changes in the growth of surface oxide films were also observed.

## ACKNOWLEDGEMENTS

The authors acknowledge support for this work from Axcelis Technologies Inc., New Jersey Economic Development Authority, New Jersey Institute of Technology, New Jersey Nanotechnology Consortium, and The Minerals, Metals and Materials Society. We especially thank J. M. Poate for his encouragement and support of this work; T. W. Sorsch for rapid thermal oxidations; and C. Batty, K. K. Bourdelle, K. Elshot, P. Frisella, and B. L. Sopori for additional contributions.

## REFERENCES

1. B.L. Sopori, U. S. patents 5,452,396, 19 September 1995, 5,577,157, 19 November 1996, and 5,639,520, 17 Jun 1997; B.L. Sopori, *Transient Thermal Processing Techniques in Electronic Materials*, ed. N.M. Ravindra and R.K. Singh (Proceedings of 1996 TMS Annual Meeting, Symposium on Transient Thermal Processing, Warrendale, Pa., 1996), pp. 17–20.
2. R. Schindler, I. Reis, B. Wagner, A. Eyer, H. Lautenschlager, C. Schetter, W. Warta, B. Hartiti, A. Slaoui, J.C. Muller, and P. Siffert, Twenty Third Photovoltaic Specialists Conference (IEEE, 1993), p. 162.
3. S. Noël, L. Ventura, A. Slaoui, J.C. Muller, B. Groh, R. Schindler, B. Fröschle, and T. Theiler, *Appl. Phys. Lett.* 72, 2583 (1998).
4. R. Singh, K.C. Cherukuri, L. Vedula, A. Rohatgi, and S. Narayanan, *Appl. Phys. Lett.* 70, 1700 (1997).
5. R. Singh, S. Sinha, R.P.S. Thakur, and P. Chou, *Appl. Phys. Lett.* 58, 1217 (1991).
6. R. Singh, M. Fakhruddin, and K.F. Poole, *Appl. Surf. Sci.* 168, 198 (2000).
7. J. Mavoori, R. Singh, S. Narayanan, and J. Chaudhuri, *Appl. Phys. Lett.* 65, 1935 (1994).
8. B. Lojek, R. Whiteman, and R. Ahrenkiel, Proceedings of RTP 2001 (RTP2001 and IEEE), p. 125.
9. B. Lojek, *Workshop on Thermal Processing of Silicon: Diffusion and Thermal Budget*, 10th IEEE Conf. on Adv. Thermal Processing of Semicond. (IEEE, 24 September 2002) p. 1.
10. R.B. Fair and S. Li, *J. Appl. Phys.* 83, 4081 (1998).
11. Y. Ishikawa and M. Maruyama, *Jpn. J. Appl. Phys.* 36, 7433 (1997).
12. S. Venkataraman, R. Singh, V. Parihar, K.F. Poole, A. Rohatgi, V. Yeludur, and A. Ebon, *J. Electron. Mater.* 28, 1394 (1999).
13. R. Ditchfield, D. Llera-Rodríguez, and E.G. Seebauer, *Phys. Rev. B: Condens. Matter Mater. Phys.* 61, 13710 (2000).
14. M.Y.L. Yung and E.G. Seebauer, Proceedings of RTP 2002 (RTP2002 and IEEE), p. 133; Symposium Q1, *Rapid Thermal and Other Short-Time Processing Technologies III*, 201st ECS Meeting, Philadelphia, May 12–17, 2002, paper 743; Fourth International Workshop on Junction Technology IWJT'04 (IEEE, 2004), p. 87.
15. R.V. Nagabushnam, R.K. Singh, and S. Sharan, *Mater. Sci. Semicond. Process.* 1, 207 (1998).
16. S. Noël, L. Ventura, A. Slaoui, J.C. Muller, B. Groh, R. Schindler, B. Froeschle, and T. Theiler, *J. Electron. Mater.* 27, 1315 (1998).
17. S. Peters, Ph.D. thesis, University of Konstantz (2004).
18. S. Peters, P.-E. Hickel, J. Horzel, S. Noel, and R. Preu, 19th European Photovoltaic Solar Energy Conference, Paris, 7–11 June 2004.
19. D. Mathiot, A. Lachiq, A. Slaoui, S. Noel, J.C. Muller, and C. Dubois, *Mater. Sci. Semicond. Process.* 1, 231 (1998).
20. A.T. Fiory, A. Agarwal, and A. Stevenson, Abstract N6.5, Symposium N, Novel Materials and Processes for Advanced CMOS (Materials Research Society, Dec 2–4 2002, http://www.mrs.org/s_mrs/bin.asp?CID=2109&DID=91224&DOC=FILE.PDF), p. 347.
21. M. Rabus, A.T. Fiory, N.M. Ravindra, P. Frisella, A. Agarwal, T. Sorsch, J. Miner, E. Ferry, F. Klemens, R. Cirelli, and W. Mansfield, *J. Electron. Mater.* 35, 877 (2006).
22. B. Nguyenphu and A.T. Fiory, *J. Electron. Mater.* 28, 1376 (1999).
23. J.P. Hebb and K.F. Jensen, *J. Electrochem. Soc.* 143, 1142 (1996).
24. L.H. Nguyen, W. Dietl, J. Niess, and Z. Nényei, 7th International Conference of Advanced Thermal Processing of Semiconductors RTP'99 (1999), pp. 26–38.
25. P.J. Timans, *Advances in Rapid Thermal and Integrated Processing*, ed. F. Roozeboom (Dordrecht: Kluwer, 1996), Chapt. 2, pp. 35–101.
26. B.J. Pawlak, R. Duffy, T. Janssens, W. Vandervorst, S.B. Felch, E.J.H. Collart, and N.E.B. Cowern, *Appl. Phys. Lett.* 89, 062102 (2006).
27. R. Kasnavi, P.B. Griffin, and J.D. Plummer, 2000 VLSI Symposium, Digest of Technical Papers (IEEE, 2000), pp. 112–113.
28. W. Aderhold, A. Jain, M. Foad, and A. Mayur, 2000 Conference on Ion Implantation Technology (IEEE, 2000), pp. 199–202.
29. H. Mikoshiba and H. Abiko, *IEEE Electron. Device Lett.* 3, 190 (1986).

30. A.T. Fiory, S.G. Chawda, S. Madishetty, V.G. Mehta, N.M. Ravindra, S.P. McCoy, M.E. Lefrançois, K.K. Bourdelle, J.M. McKinley, H.-J.L. Gossmann, and A. Agarwal, *J. Electron. Mater.* 31, 999 (2002).
31. P.M. Fahey, P.B. Griffin, and J.D. Plummer, *Rev. Mod. Phys.* 61, 289 (1989).
32. A. Mokhberi, P.B. Griffin, J.D. Plummer, E. Paton, S. McCoy, and K. Elliott, *IEEE Trans. Electron. Devices* 49, 1183 (2002).
33. A.T. Fiory and K.K. Bourdelle, *Appl. Phys. Lett.* 74, 2658 (1999).
34. N.E.B. Cowern, B. Colombeau, J. Benson, A.J. Smith, W. Lerch, S. Paul, T. Graf, F. Cristiano, X. Hebras, and D. Bolze, *Appl. Phys. Lett.* 86, 101905 (2005).
35. W.E. Beadle, J.C.C. Tsai, and R.D. Plummer, *Quick Reference Manual* (New York: Wiley, 1985), Chapt. 2.
36. A. Ural, P.B. Griffin, and J.D. Plummer, *J. Appl. Phys.* 85, 6440 (1999).